Carbohydrate Polymers 94 (2013) 634–641

Contents lists available at SciVerse ScienceDirect

Carbohydrate Polymers

journal homepage: www.elsevier.com/locate/carbpol

Construction of hyaluronic acid noisome as functional transdermal nanocarrier for tumor therapy

Ming Kong[a,*,1], Hyunjin Park[b,1], Chao Feng[a], Lin Hou[a], Xiaojie Cheng[a], Xiguang Chen[a,*]

[a] College of Marine Life Science, Ocean University of China, Yushan Road, Qingdao 266003, Shandong Province, China
[b] Graduate School Biotechnology, Korea University, 1,5-Ka, Anam-Dong, Sungbuk-Ku, Seoul 136-701, South Korea

ARTICLE INFO

Article history:
Received 19 November 2012
Received in revised form 9 January 2013
Accepted 24 January 2013
Available online 8 February 2013

Keywords:
Hyaluronic acid
Niosome
Transdermal
Tumor therapy

ABSTRACT

To develop a functional nanosized transdermal drug delivery system for tumor therapy, amphiphilic hyaluronic acid (HA) based niosome was constructed combining transdermal and tumor targeting ability in one entity. HA esterified with monostearin, the conjugate labeled as HA–GMS self-assembled onto niosome surface and formed HA–niosome. The multilayer vesicle had small size (around 40 nm), good stability and desirable drug encapsulating efficacy, and well compatible with blood. It exhibited better endocytosis to mouse breast tumor cell (4T1) than the control chitosan nanoparticle, which was verified qualitatively and quantitatively. Skin permeation of HA–niosome was proven to be efficient using in vitro stratum corneum model and in vivo fluorescence observation. Histological section study confirmed the security and efficiency of transdermal permeation. The results evidence HA–niosome to be exciting and promising for tumor therapy through trandermal administration.

1. Introduction

Carrier-mediated drug delivery has long been the interest to improve the efficacy of existing therapeutics. By virtue of small size, peculiar surface characteristics, unique physico-chemical and biological effects, numerous nanocarrier based drug delivery and drug targeting systems are currently developed or under development (Bang, Yu, Hwang, & Park, 2009; Liu & Park, 2009; Sonneville-Aubrun, Simonnet, & L'Alloret, 2004; Xia, Li, & Nel, 2009). They are tailored to enhance the in vivo efficiency of many drugs, especially anti-cancer drugs, with target to minimize drug degradation upon administration, prevent undesirable side effects, and increase drug bioavailability and the fraction of the drug accumulated in the target site (Torchilin, 2007). Conventional drug administration using nanocarrier, i.e. oral and intravenous injection (iv), offer good performance on efficacy though, its high administration frequency, low patients compliance and hepatic toxicity still need to be settled in practice.

Transdermal drug delivery (TDD) is a route of administration that drugs are delivered across the skin for systemic distribution. It is a manner to achieve drug input over extending periods of time at essentially sustained and controlled rates (Guy, 2007). TDD represents an attractive alternative to oral delivery and hypodermal injection (Prausnitz & Langer, 2008), which has been proven beneficial in reducing dose frequency, achieving target delivery and avoiding hepatic first pass metabolism (Mitragotri, 2004). The administration is easier and able to be suspended if necessary. Furthermore, steady absorption of drug over hours or days is usually preferable to the blood level spikes and troughs produced by oral dosage forms (Subedi, Oh, Chun, & Choi, 2010). Potential nanocarriers for TDD involve microemulsions (MEs), vesicles and nanoparticles (Neubert, 2011). Since non-compressible and rigid structure, nanoparticles are unable to cross pores comparable to or smaller than their own diameter (Cevc & Vierl, 2010). Even though MEs have substantial penetration enhancing effects for extremely lipophilic drugs in colloidal phase, the large content of surfactants causes severe irritation to skin (Santos, 2008). Owing to bilayer elasticity and transformable peculiarity, vesicular (liposomal) carriers turn out to be the most popular (Cevc & Vierl, 2010). Major advantage ascribed to their amphipathic nature, which allows the incorporation of both hydrophilic and hydrophobic drugs (Pham, Jaafar-Maalej, Charcosset, & Fessi, 2012).

Niosomes and liposomes are two representative vesicles made of non-ionic surfactants and phospholipids, respectively. In spite of liposomes could be of great interest for drug delivery, there are shortcomings associated with their physico-chemical stability (phospholipid hydrolysis or oxidation), high cost in production and variable purity of natural phospholipids. Besides, drug entrapment efficiency of liposomes is less than niosomes due to cholesterol content (Kazi et al., 2010). Noisome are non-ionic surfactant vesicles obtained on hydration of synthetic nonionic surfactants, with

* Corresponding authors at: 5# Yushan Road, Ocean University of China, Qingdao 266003, China. Tel.: +86 532 82032586; fax: +86 532 82032586.
E-mail addresses: kongming@ouc.edu.cn (M. Kong), xgchen@ouc.edu.cn (X. Chen).
[1] The author contributed equally to this study with the first author.

0144-8617/$ – see front matter © 2013 Elsevier Ltd. All rights reserved.
http://dx.doi.org/10.1016/j.carbpol.2013.01.091

Table 1
Characteristics of HA–GMS conjugates and HA–N.

HA–GMS	HA (kDa)	DS (%)[b]	Size (nm)	PdI	ξ (mV)[c]	E.E. (%)[d]
H6.5[a]	110	7	47.2 ± 0.2	0.46	−23.77 ± 2.21	56.5 ± 3.6
H14	110	14	46.0 ± 0.3	0.44	−22.51 ± 1.67	–
H23	110	23	44.2 ± 0.3	0.45	−20.39 ± 2.43	72.4 ± 2.5
L6	10	6	38.2 ± 0.4	0.37	−20.24 ± 1.98	94.3 ± 1.2
L22	10	22	36.3 ± 0.2	0.39	−17.83 ± 1.83	–

[a] Capitals denoted M_w property of HA and numbers were DS of HA–GMS.
[b] DS, defined as the number of GMS molecules per 100 sugar residues of HA.
[c] The ξ potential of HA–N (1 mg/mL) in PBS (7.4).
[d] E.E. was calculated as the percentage of ratio of encapsulated VE mass to total VE mass (1 mg/mL).

or without incorporation of cholesterol or other lipids, which are biodegradable, relatively nontoxic, more stable and inexpensive, an alternative to liposomes (Patel, 2007). Slow penetration of drug through skin is the major drawback of transdermal route of delivery (Jayaraman, Ramachandran, & Weiner, 1996). Transdermal delivery of drug incorporated in niosomes results in enhanced delivery of drugs through the stratum corneum, and the delivery would be specifically enhanced if in combination of hydrophilic surfactants, which generate flexible bilayer flexible for "elastic" vesicles (Torchilin, 2007).

Hyaluronic acid (HA) is a naturally occurring polymer. Owing to its biocompatibility and biodegradability, HA has been extensively investigated for biomedical applications. HA derivatives acquire additional physicochemical characteristics besides their inherently superior properties. Amphiphathic derivatives endow HA with ability to be active in surface arrangement and colloidal edge adjustment (Kong, Chen, & Park, 2011). Moreover, HA can specifically bind to various cancer cells that over-express CD44, offering targeting ability to tumor for anti-cancer therapeutics (Choi et al., 2010). In addition, stabilin 2, HA receptor for endocytosis protein, promotes the uptake by tumor cells (Harris & Weigel, 2008). In this study, a novel drug nanocarrier HA niosome was developed, which combined transdermal delivery and tumor targeting together. Concerning physicochemical characteristics and biocompatibility were studied. In vitro and in vivo transdermal activities were evaluated qualitatively and quantitatively. 4T1 cell line was used to assess the endocytosis of HA niosome labeled by FITC.

2. Materials and methods

2.1. Materials

Sodium form of HA (M_w, 110 and 10 kDa) was a gift of Kolon Life Science, Korea. EDC·HCl (99%) and N-hydroxy succinimide (NHS, 99%) were purchased from Shanghai Medeep Co., Ltd. Monostearin (glycerol α-monostearate, GMS), ethylenediamine (EDA) were purchased from Tianjin Chemical Reagent. Methylene chloride, sodium bromide, Triton X-100 and acetonitrile (HPLC grade) were purchased from Huasheng Chemical. α-tocopherol (97%) (Vitamin E, VE), fluorescein isothiocyanate (FITC), POE (20) sorbitan monooleate (Tween 80) and sorbitan monolaurate (Span 20) were purchased from Sigma. Tissue-Tek® O.C.T™ Compound was ordered from Sakura Finetek USA, Inc. Water, used for synthesis and characterization was purified by distillation, deionized and subjected to reverse osmosis using a Milli-Q Plus apparatus (Millipore, USA). All the chemicals were analytical grade and were used as received.

2.2. Preparation of HA–GMS and FITC labeled HA–GMS

Different batches of amphiphilic HA–GMS were synthesized by a previous method (Kong, Chen, & Park, 2011), as shown in Table 1. Briefly, GMS was conjugated to HA by the formation of ester linkages through an EDC-mediated reaction. HA (190 mg) and EDC/NHS were dissolved in PBS at 1:1:1 mole ratio and maintained for 2 h. The solution was then added to GMS (60–540 mg) acetone solution dropwise with magnetic stirring (IKA RO10, Germany). The resultant mixture was centrifuged (15,000 rpm, 20 min) and the apparent solution was extensively dialyzed and lyophilized. The degree of substitution (DS) of GMS was determined by ^{1}H NMR, and was calculated from the ratio of the relative peak integrations of the GMS ending methyl protons (peaks at around approximately 1.0 ppm) and methyl protons in HA acetamide (approximately 2.0 ppm) (Kong, Chen, & Park, 2011). The obtained HA–GMS conjugate was dissolved in formamide along with EDC/NHS at molar ratio of 1:12:12 allowing for 2 h reaction. The solution was added dropwise into EDA, the free mole ratio of HA–GMS and EDA was about 1:200. After reaction for 6 h, the EDA–HA–GMS was dialyzed against water for 48 h. Ethanol solution of FITC was slowly added into EDA–HA–GMS. The reaction was ended 4 h later and dialyzed for 48 h before lyophilization.

2.3. Preparation of HA–niosome (HA–N)

HA–N was prepared by emulsion–evaporation method. HA–GMS emulsion was formed firstly based on modified protocol (Kong, Chen, & Park, 2011). Nonionic surfactants Tween 80/Span 20 (molar ratio 5:4) were dissolved in methylene chloride at proportion of 60%. The mixture (1 mL) was dispersed in 1 mg/mL HA–GMS PBS (7.4) solution with final volume of 20 mL, which was then sonicated twice (pulse on, 10.0 s; pulse off, 2.0 s), using a Sonics Vibra-Cell CV33 ultrasonic probe (Sonics & Materials, USA) at 225 W in an ice bath for 3 min. The methylene chloride was removed by a rotary vacuum evaporator at 35 °C, the suspension obtained was heated on a water bath at 60 °C for 10 min to yield HA–N. VE loading niosome was generated by dissolving VE in methylene chloride in preparation.

2.4. Characteristics of HA–N

Size analysis and zeta potential were determined on a Zetasizer ZEN 3600 Nano Series apparatus (ZEN, UK).

The morphology of HA–N was observed via a transmission electron microscope (TEM, JEM-1200EX JEOL Ltd., Japan).

VE loading niosomes were firstly purified by Sephadex G25 fine column. The amount of loaded VE was measured by HPLC at 280 nm using a reversed phase C18 column (Nova-Pak® C18, 3.9 mm × 150 mm, Waters Associates) operated at room temperature, a Waters 2690 Separation Module (Waters Associates) and a Waters 996 photodiode Array Detector (Waters Associates). Acetonitrile (HPLC grade) was used as eluent at a flow rate of 1 mL/min. Encapsulation efficiency (E.E.) was calculated as the percentage of ratio of encapsulated VE mass to total VE mass.

2.5. In vitro hemolysis assay

Hemolysis assay was performed using citrated whole blood obtained from healthy male New Zealand white rabbit. Erythrocytes were separated by centrifugation (1500 × *g*, 10 min), rinsed and resuspended with PBS (pH 7.4) to attain 2% (w/w) erythrocytes stock dispersion. The stock was supposed to be stored in 4 °C and used within 24 h. The approximate amount of red blood cell was 3.75×10^8 cells/mL. 1 mL noisomes of series concentrations were added to 0.5 mL erythrocyte stock dispersion. After incubation for 1 h, unlysed erythrocytes and debris were removed by centrifugation (1500 × *g*, 10 min), and absorbance of the supernatant was measured at 540 nm on UV1200 UV/vis spectrophotometer (Mapada, China). The hemolysis elicited by the Triton X-100 solution (5%) was designated to be 100% while the hemolysis given by the PBS (pH 7.4) was taken as 0%. The hemolysis rate (HR%) was calculated by Eq. (1):

$$\mathrm{HR\%} = \frac{\mathrm{Dt} - \mathrm{Dnc}}{\mathrm{Dpc} - \mathrm{Dnc}} \times 100\% \quad (1)$$

where Dt, Dnc, and Dpc are the absorbances of the tested sample, the negative control, and the positive control, respectively.

2.6. In vitro cellular uptake of HA–N

The quantitative study was investigated according to literature (Khin & Feng, 2005). Mouse mammary tumor cell line 4T1 cells were cultured in DMEM (Gibco, Grand Island, NY, USA) containing FBS (10%) and penicillin–streptomycin (100 U/mL culture medium) at 37 °C in a 5% CO_2 humid atmosphere. After cell attachment, the medium was replaced by HBSS (pH 7.4) and equilibrated for 30 min. Fresh prepared FITC–HA–N with HBSS (50, 25, 12.5 μg/mL) were replenished, followed by incubation for 0.5, 1 and 2 h, respectively. Cell samples without treatment of FITC–HA–N were taken as negative control. The cells were then washed twice with PBS (pH 7.4) and treated by 0.5% Triton X-100 for 30 min to lyse the cells. The amount of endocytosed FITC–HA–N was measured by fluorescence plate reader (Bio-Tek Instruments, λ_{ex} 485 nm, λ_{em} 528 nm). Calibration curve was constructed of FITC fluorescence intensity as function of FITC–HA–N with serial concentrations. Cellular uptake ratio (UR%) was calculated by Eq. (2):

$$\mathrm{UR\%} = 100 \times \frac{C_\mathrm{u}}{C_\mathrm{i}} \quad (2)$$

Hereinto, C_u and C_i were the uptake and initial concentrations of FITC–HA–N, respectively.

Microscopic observation was conducted referred to Zhang (Zhang et al., 2004). After cell attachment and HBSS equilibration, 50 μg/mL FITC–HA–N was added to the medium, allowed for incubation for 0.5 and 1 h, hereinto, 50 μg/mL FITC labeled chitosan (CS) nanoparticle was utilized as control to evaluate HA's enhancing endocytosis. The intracellular localizations of HA–N and CS–NPs were observed using inverted fluorescence microscope (Nikon Eclipse Ti-S, Nikon Ltd., Japan), in which the excitation and emission wavelengths were 485 nm and 528 nm, respectively.

2.7. In vitro stratum corneum (SC) permeation of HA–N

2.7.1. Skin separation

Kunming mice (male, 20–25 g, Qingdao Municipal Institute for Drug Control, China) were taken to study the transdermal penetration of HA–N. The study was conducted in accordance with the guidelines of University laboratory Animal ethical Committee. Hairs on dorsal skin were removed with lab-made hair removal solution a day before experiment. The mice were sacrificed by cervical dislocation. The full thickness dorsal skin was excised and subcutaneous tissues were carefully removed with surgical scissors. The skin samples were treated with 2 M sodium bromide solution for 90 min. The skin was treated with 2 M sodium bromide solution in distilled water for 90 min at 25 °C. The SC from full thickness skin was separated using cotton swab moistened with water. SC sheet was cleaned by rinsing with PBS and blotted to dry and examined for cuts or holes if any. SC samples were spread carefully and identified the epidermal and dermal sides, packed with aluminum foil and stored at −4 °C till further use within 24 h (Kong, Chen, Kweon, & Park, 2011).

2.7.2. Skin permeation study

Skin permeation studies were performed on modified static-type amber Franz cells (diameter 14 mm, volume 10.76 mL, Daihan Labtech Co., Ltd., South Korea). The SC sheets were placed between the donor and acceptor chambers of the diffusion cells with the epidermal side facing upwards. The excess skin was trimmed off and the acceptor chambers were filled with degassed PBS (pH 7.4). The acceptor phase was stirred magnetically to equilibrate for 30 min at 37.2 °C. 2 mL HA–N (1.0 mg/mL), loaded with VE (1.0 mg/mL), was added to donors and the acceptor chambers were filled with fresh PBS (7.4). VE ethanol solution (1.0 mg/mL) was taken as control group. 1 mL samples were withdrawn at intervals (0.5, 1, 2, 4, 6 and 8 h) and replenished with fresh degassed PBS. The whole process of manipulation should avoid formation of bubbles. The samples were filtered through 0.45 mm membrane filter and analyzed for drug content by HPLC as mentioned in Section 2.4.

2.7.3. Data analysis

Cumulative active ingredient penetration (Qt, μg/cm^2) through the skin was calculated from the following equation (Sintov & Shapiro, 2004):

$$\mathrm{Qt} = V_\mathrm{r} C_\mathrm{t} + \sum_{i=0}^{t-1} V_\mathrm{s} C_\mathrm{i} \quad (3)$$

where C_t is the drug concentration of the acceptor phase at each sampling time, C_i is the drug concentration of the *i*th sample, and V_r and V_s are the volumes of the acceptor solution and the sample, respectively. Data were expressed as the cumulative drug permeation per unit of skin surface area, Qt/*S*. The steady-state fluxes (Jss, mg/cm^2 h) were calculated by linear regression interpolation of the experimental data at a steady state:

$$\mathrm{Jss} = \frac{\Delta \mathrm{Qt}}{\Delta t \times S} \quad (4)$$

Apparent permeability coefficients (Kp, × 10^{-3} cm/h) were calculated according to the equation:

$$\mathrm{Kp} = \frac{\mathrm{Jss}}{C_\mathrm{d}} \quad (5)$$

where C_d is the active ingredient concentration in the donor chamber, and it assumed that under sink conditions the drug concentration in the acceptor chamber is negligible compared to that in the donor chamber.

2.8. In vivo skin permeation of HA–N

2.8.1. Fluorescence observation

Male Kunming mouse was taken as model to study the transdermal penetration of HA–N. Hairs on dorsal skin were removed with lab-made hair removal solution a day before administration. Lab-made non-occlusive containers (diameter 5 mm, volume 0.2 mL), simulating Franz diffusion donor cell, were adhered on the hairless skin. FITC–HA–N was added at dose of 2.5 mg/kg into the donor cells, leaving the permeation last for 2 or 8 h, respectively. Full

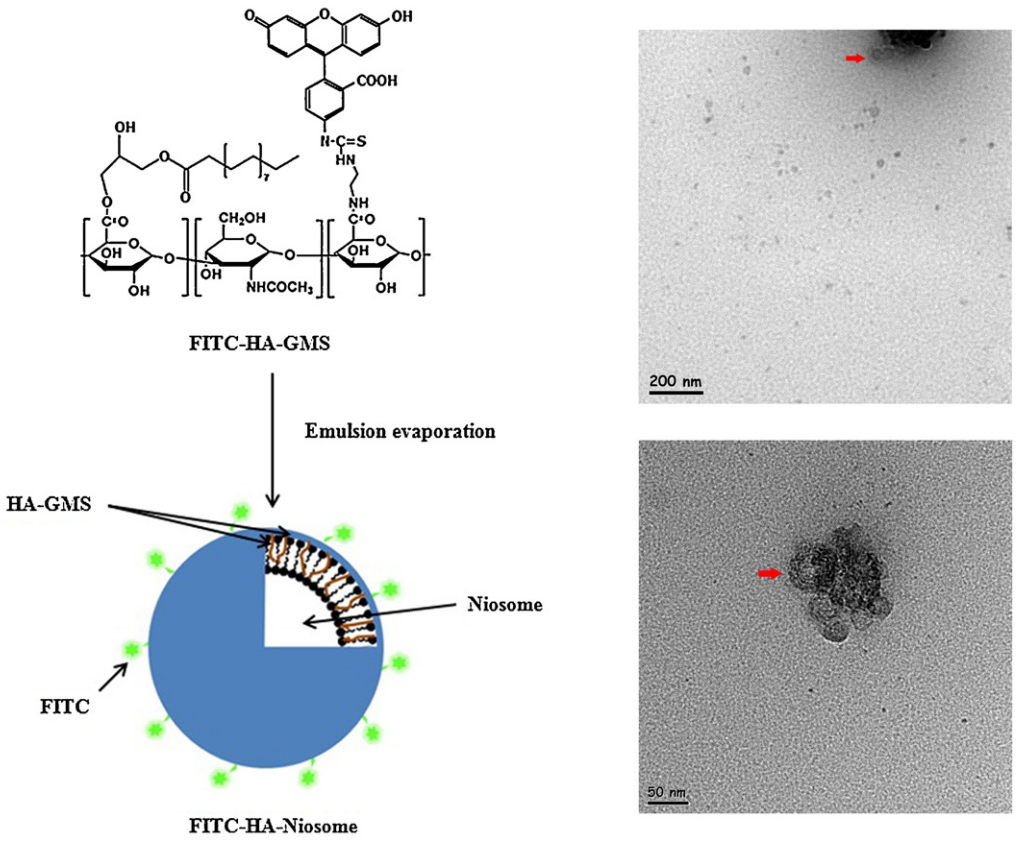

Fig. 1. Structure of FITC labeled HA–niosome and its transmission electrograph.

thickness skin tissue were excised when administration ended, rinsed with PBS (7.4) to clear off the remaining formulations and frozen at −20 °C. Cryotome sections of 30 μm thickness (Thermo Scientific Cryotome FSE, Germany) were subjected to inverted fluorescence microscope using FITC filter (Nikon Eclipse Ti-S, Nikon Ltd., Japan) and the camera integration time was set to 1 s.

2.8.2. Histological examination

Part of the excised full thickness skin tissues treated with HA–N was fixed by 10% polyformaldehyde. The skin samples were dehydrated using ethanol, replaced ethanol with xylene, embedded in paraffin for fixing, subjected to paraffin vertical sections (Thermo Scientific Microm HM 340 E Rotary Microtome, Germany), and stained with hematoxylin and eosin. These samples were then observed under light microscope (Olympus CX40 equipped with DigiCAM II, Olympus, Japan) and compared with the control sample that was free of HA–N administration.

2.9. Statistics

All statistical evaluations were performed by OriginPro 8.0 (OriginLab Corporation, Northampton, MA, USA). Statistical significance was found by One-Way ANOVA, Tukey test was used to analyze differences. The presented data (arithmetic mean value ± standard deviation) resulted from at least three independent experiments ($n \geq 3$), the value of $p < 0.05$ was considered as significant.

3. Results and discussion

3.1. Characteristics of HA–Ns

HA was modified with GMS to acquire assembling ability as to be active in interface arrangement, like being assembled onto the surface of vesicles, and thus giving rise to multifunctional nanocarriers (Fig. 1). The DS of HA–GMS samples accordingly make sense on determining their assembling behaviors through modulating hydrophobic property. Among five batches of samples (H6.5, H14, H23, L6 and L22, hereinto, capitals denoted M_w property of HA and numbers were DS of HA–GMS.), as for same M_w HA, higher value of DS tended to form smaller HA–N as expected (Table 1), which resulted from the stronger hydrophobicity. H23 and L22 had smaller size on their individual M_w level, for instance. Moreover, low M_w HA gave smaller size than high M_w, L22 gave HA–Ns with the smallest size. The sizes of HA–N were well in accordance with the hydrophobicity of HA–GMS, which descended in order as H6.5, H14, H23, L6 and L22 (Kong & Park, 2011).

Zeta potential absolute value of HA–N increased with the increasing hydrophilicity of HA–GMS. Since the negative charges derived from carboxylic groups of HA as detecting pH was below its isoelectric point (pI = 2.5), rising DS led to decreasing amount of free carboxyl. It followed that L22 comparatively exhibited poor solubility and lack of systemic stability in niosome formulation.

Three typical HA–Ns involving gradient hydrophobicity, H6.5, H23 and L6 were selected for E.E. assessment. As shown in Table 1, E.E. of the three samples are 56.5 ± 3.6%, 72.4 ± 2.5% and 94.3 ± 1.2%, respectively, coinciding with the tendency of hydrophobicity of the samples. It was reported that niosome made of span 60 behaved the best in E.E. in comparison with the formulations derived from span 20 and 40, arising from the longest alkyl chain of span 60 (Hao, Zhao, Li, Yang, & Li, 2002), which probably imparted it with the strongest hydrophobicity. This speculation is also suitable for HA–N that L6, as expected, exhibited the highest efficiency of loading capacity.

TEM photos displayed apparent multilayer vesicular structure of HA–N, marked in Fig. 1, which provided HA–N with distinct loading capacity. The vesicles had spherical morphology and uniform size distribution that were less than 50 nm in size. It was demonstrated

that emulsion–evaporation method could be utilized to formulate small size multilayer niosome.

3.2. In vitro hemolysis study

In vitro hemolysis was found to be concentration dependent as treated with HA–N, and HR% rose up with raising concentration of HA–N (Fig. 2). 5% is typically taken as the upper limit for hemo-compatible material assessment (Rao & Sharma, 1997). According to this criterion, among the formulations, H23 turns out to be potentially hemolytic one due to 6.18% breakdown of hemoglobin at treating concentration of 1 mg/mL. Comparatively, both H6.5 and L6 behaved well within the permitting limit under either concentration, ranging from 0.88% to 3.65% and 1.46% to 2.63%, respectively. L6 was relatively the most hemocompatible one, whose hemolytic level was significantly lower than another two formulations ($p \leq 0.05$).

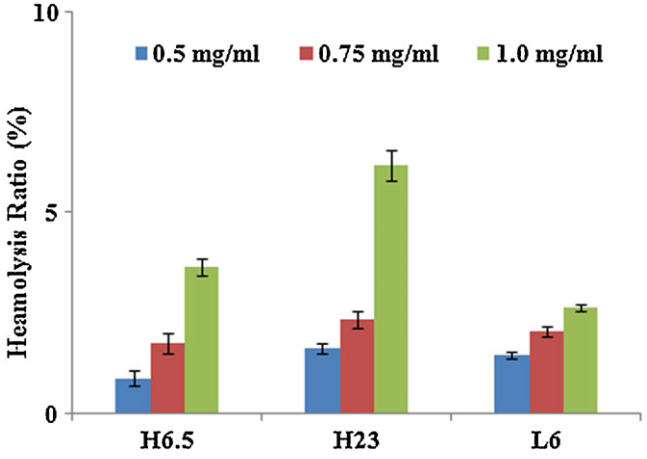

Fig. 2. The effects of different concentrations and formulation of the HA–N on hemolysis ratio (%) after 1 h incubation. Mean ± SD ($n = 3$) of the data in each group are shown in each bar. Triton X-100 (5%, v/v) was considered as the positive control and PBS (pH 7.4) as negative control.

3.3. In vitro cellular uptake

The tumor growth and metastatic spread of 4T1 cells in mice very closely mimic human breast cancer, which therefore was taken as model and underwent exposure to FITC–HA–N. L6, owing to its superior activity, was chosen as testing formulation, while CSNP prepared by ionic gelation was designated as non-receptor mediated endocytic control formulation in this experiment. Quantitative study was carried out as function of concentration and treating time (Fig. 3A). Similar trends appeared for each concentration, which rose after 0.5 h incubation, peaked at 1 h and decreased afterwards. The time dependence attributed to cellular uptake that was

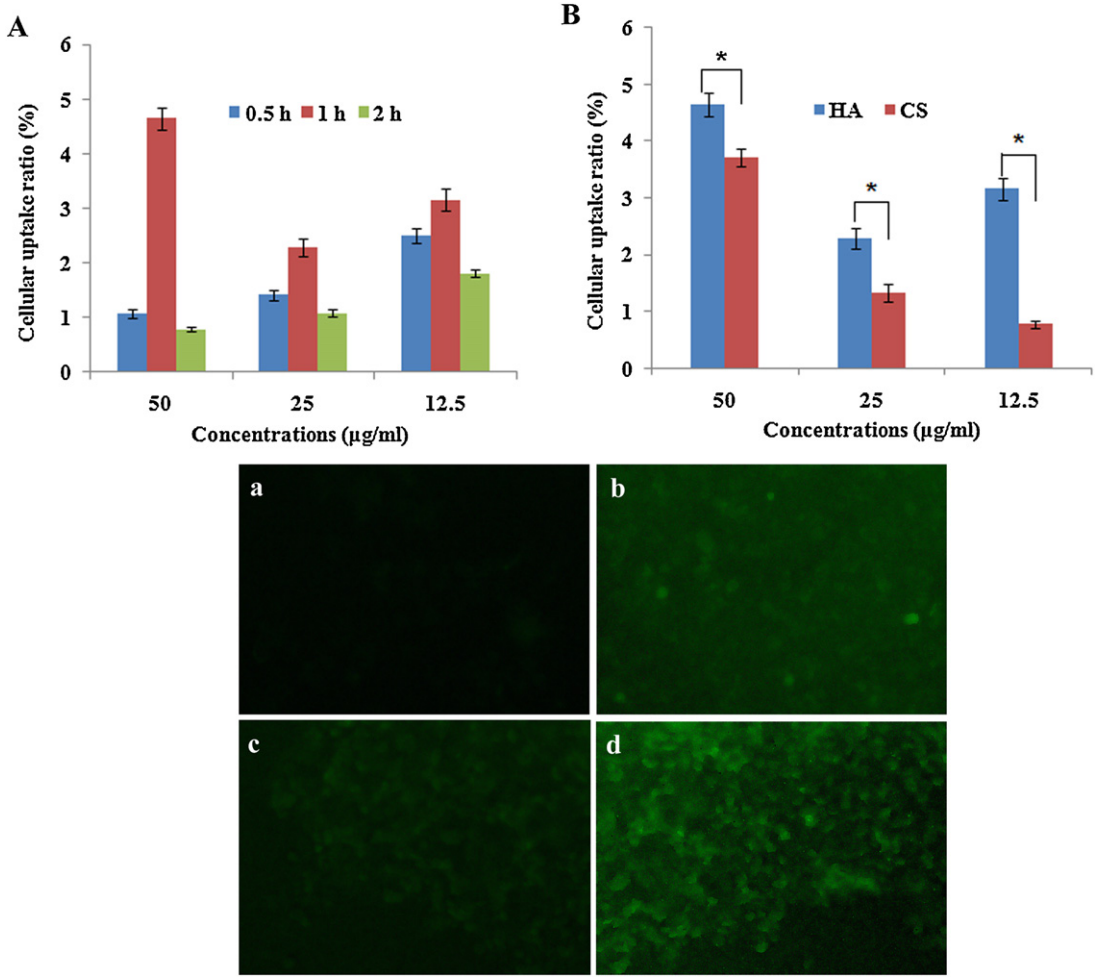

Fig. 3. Upper panel: cellular uptake ratio by mammary tumor cell line 4T1 cells as function of FITC–HA–N (L6) incubation time and concentrations (A), different formulations (FITC–HA–N and FITC–CSNP) and concentrations (B). The p-values were obtained by One-Way ANOVA ($p \leq 0.05$). Bottom panel: microscopic fluorescent observation (40×) of cellular uptake ratio by mammary tumor cell line 4T1 treated with: 50 μg/mL FITC–CSNP for 0.5 h (a) and (b) 1 h, 50 μg/mL FITC–HA–N for (c) 0.5 h and (d) 1 h, respectively.

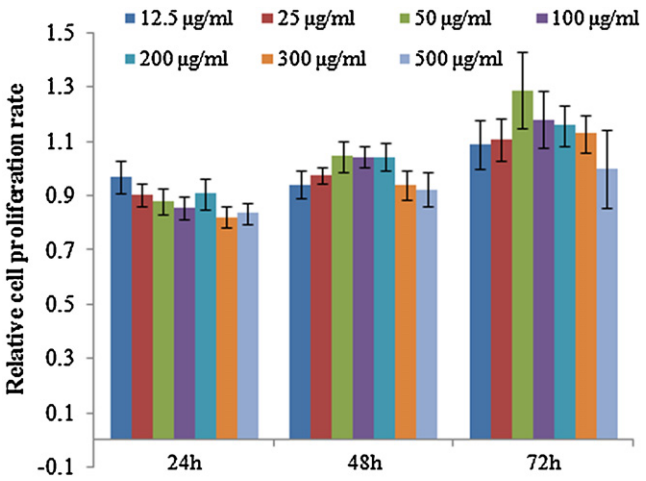

Fig. 4. The effects of HA–N (L6) on relative cell proliferation rate under various concentrations and incubation period.

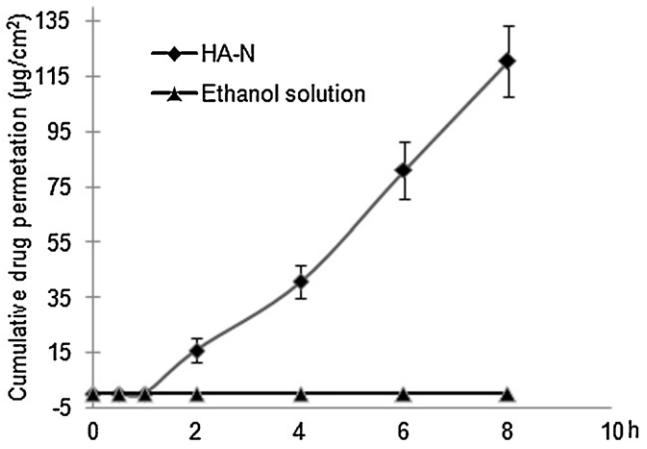

Fig. 5. In vitro permeation profiles of vitamin E through the excised mice dorsal skin from 1.0 mg/mL HA–N (L6). The control sample was ethanol solution of VE (1.0 mg/mL) (mean ± S.D., $n = 5$).

a dynamic process as long as the cells were in good condition, which were supposed to have been endocytosing until equilibrium. It suggested that the 4T1 cells displayed good state at least in the first 1 h. The later steep descent maybe arose from cytotoxicity of HA–N given by the nonionic surfactants in niosome. Relative cell proliferation rate using human umbilical vein endothelial cells (HUVECs) of L6 itself without surfactants was determined by MTT assay (Fig. 4). All the tested concentrations ranging from 12.5 to 500 μg/mL allowed at least 82.1% cell to survive compared with the control, indicating good cytocompatibility of HA–GMS. The result supports the hypothesis that the source of toxicity coming from the incorporation of surfactants.

Surfactants are typically cytotoxic in nature due to their amphiphilic property, which are surface active to compromise the integrity of cell membrane. Tween 80 and Span 20 are two of the lowest toxic surfactants and wildly applied in pharmaceutical formulations (Kulkarni & Feng, 2011; Sun, Xie, Wang, & Hu, 2004). The relatively higher surfactant content (3%, m/v) than that as reported (0.5–1%) probably contributed to the increased cytotoxicity. However, it deserves to note that niosome requires larger amount of surfactant for transdermal administration than that for i.v., on one hand is to overcome stratum corneum barrier, on the other is to maintain its own deformability for permeation. In addition, TTD is a continuous slow process of diffusion into circulation rather than the intensive manner done in one shot for iv, exposure of high concentration drug in vivo could thus be avoided.

Not only did HA–N appear good ability in endocytosis, it also exhibited significantly better performance than CSNP ($p < 0.05$), which suggested the concerning receptor localized on tumor cells surface favored HA to be taken by them (Fig. 3B).

Fluorescent microscopic photo provide direct evidences of cellular uptake (Fig. 3). 4T1 treated by HA–Ns or CSNPs for 1 h (Fig. 3b and d) displayed higher fluorescence intensity than 0.5 h, only faint shadow appeared for CSNPs at 0.5 h (Fig. 3a). Meanwhile, HA–Ns showed stronger lightness in the process (Fig. 3c and d). The results are well accordant with the quantitative study.

3.4. In vitro stratum corneum (SC) permeation

Based on the small size, bioactive properties and high encapsulation capacity of drug, L6 was taken as tested formulation in skin penetration experiment. VE ethanol solution (1.0 mg/mL) was taken as control group and PBS (pH 7.4) as acceptor phase. As shown in Fig. 5, the cumulative amount of VE detected in acceptor phase increased with treating time after a lag period (0–1 h) and reached final concentration of 17.89 μg/mL. The permeation profile displayed typically approximate linearity. The transport of molecules across the skin through passive diffusion means that the solute flux was linearly dependent on the solute concentration gradient (Potts & Francoeur, 1991; Scheuplein, 1976). For in vitro skin penetration test via passive diffusion, sink condition regarding acceptor concentrations ≤10% of the donor concentrations is a prerequisite demand to be met to attain a desirable permeation profile (Kong, Chen, Kweon, et al., 2011). In this study, VE concentration in acceptor at 8 h accounting for 1.98% of donor concentration indicated sink condition was well achieved. Otherwise, the SC permeation flux was supposed to further increase until equilibrium if the permeation was not ended.

The whole process resulted in VE steady-state flux (Jss) of 21.30 ± 4.23 μg/cm^2 h. Compared with HA nanomeulsion in previous study (Kong, Chen, Kweon, et al., 2011) that has exerted excellent transdermal capacity known by lower donor concentration and content of surfactant than its category, HA–N created 1.45-fold higher flux. First of all, the structural attributes of niosome as elastic vesicle, involving more deformable mobility and better membrane fluidity, favor it to lower skin barrier and enhance permeation (Honeywell-Nguyen & Bouwstra, 2005), whereas HA nanoemulsion has single layer of surfactant in aqueous phase, born with relatively rigid structure. In addition, the small vesicle size most likely made certain contribution for efficient permeation. Given that normal stratum corneum only contains pores with <10 nm diameter, the majority of which are smaller than 5 nm, nanosized aggregates accordingly get potential for drug delivery across skin barrier but still have to own additional ability to reduce skin barrier, like deformability as such (Cevc & Vierl, 2010). With regard to elastic vesicle, smaller size turned out to be promising for dermal delivery (Verma, Verma, Blume, & Fahr, 2003). Besides the abovementioned primary causes, the differing animal sources may also lead to the superiority of HA–N over HA nanoemulsion.

In contrast to HA–N, no presence of VE has been detected for the control group of ethanol solution over 8 h treatment. Ethanol has long been known to have permeation enhancing capacity and it disturbs the organization of the stratum corneum lipid bilayer and enhances its lipid fluidity, which results in an increase in membrane permeability (Thong, Zhai, & Maibach, 2007). Extraction of the lipids from stratum corneum also leads to enhanced skin permeation (Bommannan, Potts, & Guy, 1991). It thereby appears to be a paradox that VE ethanol solution fails to permeate through SC. Major cause probably attributes to the nature of acceptor phase PBS (pH 7.4). Passive diffusion of VE through SC is proportional to

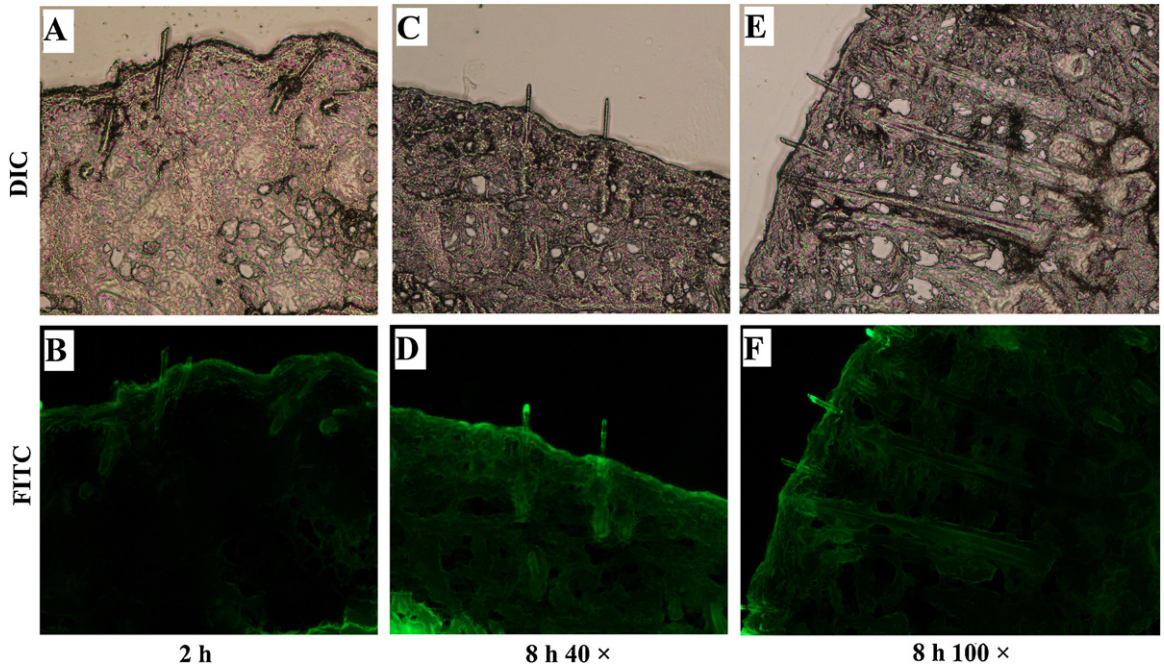

Fig. 6. In vivo permeation of 1.0 mg/mL FITC–HA–N (L6) into mice dorsal skin after 2 h treatment (A and B, 40×), 8 h treatment (C and D, 40×) and (E and F, 100×), respectively. Images were obtained in light and fluorescence mode with camera integration time was set to 1 s.

partition coefficient, which is determined by solubility between the "source" and "target" solvents. For instance, the diffusion of VE from donor solution into SC layers was favorable, because the SC shared the same polarity with VE, and VE did permeate into the SC layer. Nevertheless, between SC and acceptor phase, the insolubility of VE in PBS elicited the failure of partitioning. The VE might be stuck in SC layer rather than diffused over it. Due to high solubility, binary ethanol–water solvent was therefore wildly exploited in donor chamber to ensure perfect sink conditions for in vitro skin penetration study using lipophilic drugs (Krishnaiah, Satyanarayana, & Karthikeyan, 2002; Lee, Lee, Kim, Yoon, & Choi, 2005). In this study, PBS (pH 7.4) was used as acceptor phase to simulate the in vivo condition more suitable than ethanol–water solvent. However, the sink condition in vivo is unable to be mimicked just by PBS.

3.5. *In vivo skin permeation*

Microscopic photos of skin exposed to FITC–HA–N for 2 and 8 h offer direct evidences of permeation (Fig. 6). After 2 h treatment, FITC signal was found mostly in epidermal area (Fig. 6A and B), and SC layer emitted stronger fluorescent intensity demonstrating continuous permeation. The HA–N diffused further into deep dermis after 8 h and generated brighter signal indicated higher accumulation of permeated vesicles (Fig. 6C and D). Tissue details could be visible under high magnification. It is apparent that HA–N preferentially accumulates around hair follicles and has an even diffusion throughout the aqueous environment of the dermis and epidermis, including the vascular distribution (Fig. 6E and F). Nevertheless, neither can hydrophilic nor lipophilic drugs accomplish transdermal transport freely. Without penetration enhancer, hydrophilic molecules are rarely able to penetrate into SC layer owing to its mortar and brick structure. The things for lipophilic molecules are also not optimistic arising from their low partition coefficient between SC and deep aqueous epidermis. There are four accessible pathways: intercellular, transcellular, pilosebaceic and the polar pores pathway (Kogan & Garti, 2006). The protein and lipid regions in SC form the polar and nonpolar pathways, respectively. The transcellular route or polar pathway takes place through the hydrated

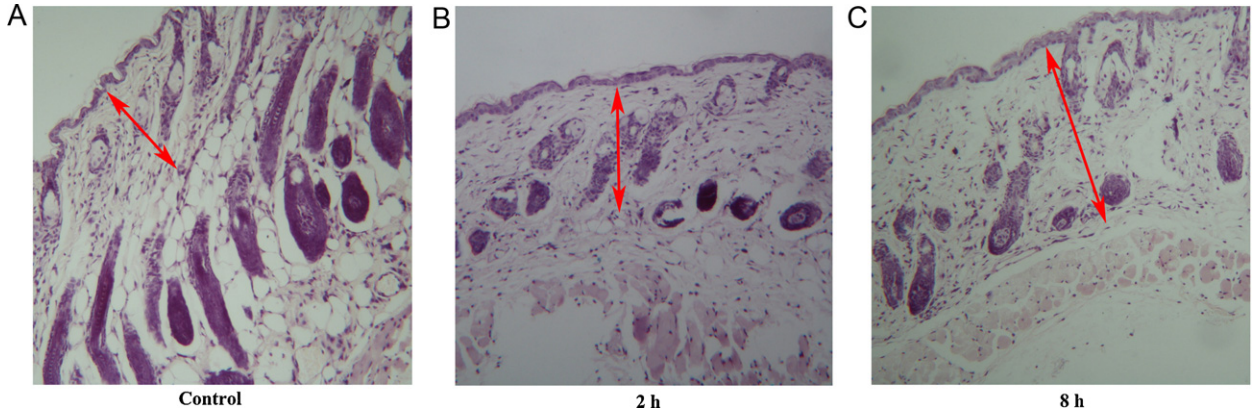

Fig. 7. Histological microimages (HE staining, 40×) of mice skin samples treated with 1.0 mg/mL FITC–HA–N (L6): control group (A), 2 h treatment (B) and 8 h treatment (C), respectively.

proteins of the keratinocytes. Along with hair follicles, both of them are the major hydrophilic accesses, through which drugs achieve transdermal permeation with favor of niosome (Fig. 6F).

3.6. Histological examinations

Dorsal skin samples were excised from mice body and stained by HE method. SC layer was intact and adjacent to the topmost of epithelium. Stratified squamous cells arranged closely comprised epithelial tissue. Sebum glands and follicles of the treated skin samples were found to be slightly shrunk compared with the control, which probably the result of lipid extraction by surfactants in niosomes (Fig. 7). No sign of skin irritation, such as inflammatory cell infiltration or erythema, has been found in dermis among tested samples. Nevertheless, expansion of collagen (labeled by arrows) and compression or receding of lipocyte in the meantime was apparent after treatment. It is well know that hyaluronic acid could hold water and give skin volume, thus forms jelly-like substance that fills the space between collagen and elastin fibers. HA–niosomes that successfully penetrated through the epithelium would play its hydrating role in presence of collagen, which was also an evidence of its transdermal ability.

4. Conclusion

HA–GMS conjugate could self-assemble onto niosome surface and form HA–niosome. Its small size, elastic multilayer structure and hydrophilic interface facilitated transdermal permeation. The incorporation of HA significantly promoted the endocytosed amount of nanocarrier by tumor cell. HA–niosome is not only efficient and secure for transdermal permeation, it also offers a useful and promising carrier for tumor therapy through percutaneous administration.

Acknowledgments

This study is supported by grant from NSFC (31240007 and 81271727) and Shandong Youth Scientist Awards Foundation (BS2012SW024).

References

Bang, S. H., Yu, Y. M., Hwang, I. C., & Park, H. J. (2009). Formation of sizecontrolled nano carrier systems by self-assembly. *Journal of Microencapsulation*, *26*, 722–733.

Bommannan, D., Potts, R. O., & Guy, R. H. (1991). Examination of the effect of ethanol on human stratum corneum in vivo using infrared spectroscopy. *Journal of Controlled Release*, *16*, 299–304.

Cevc, G., & Vierl, U. (2010). Nanotechnology and the transdermal route: A state of the art review and critical appraisal. *Journal of Controlled Release*, *141*, 277–299.

Choi, K. Y., Chung, H. J., Min, K. H., Yoon, H. Y., Kim, K. M., Park, J. H., et al. (2010). Self-assembled hyaluronic acid nanoparticles for active tumor targeting. *Biomaterials*, *31*, 106–114.

Guy, R. H. (2007). Transdermal science and technology—an update. *Drug Delivery System*, *22*, 442–449.

Hao, Y. M., Zhao, F. L., Li, N., Yang, Y. H., & Li, K. A. (2002). Studies on a high encapsulation of colchicine by a niosome system. *International Journal of Pharmaceutics*, *244*, 73–80.

Harris, E. N., & Weigel, P. H. (2008). The ligand-binding profile of HARE: Hyaluronan and chondroitin sulfates A, C, and D bind to overlapping sites distinct from the sites for heparin, acetylated low-density lipoprotein, dermatan sulfate, and CS-E. *Glycobiology*, *18*(8), 638–648.

Honeywell-Nguyen, P. L., & Bouwstra, J. A. (2005). Vesicles as a tool for transdermal and dermal delivery. *Drug Discovery Today: Technologies*, *2*(1), 67–74.

Jayaraman, S. C., Ramachandran, C., & Weiner, N. (1996). Topical delivery of erythromycin from various formulations: An in vivo hairless mouse study. *Journal of Pharmaceutical Sciences*, *85*, 1082–1084.

Kazi, K. M., Mandal, A. S., Biswas, N., Guha, A., Chatterjee, S., Behera, M., et al. (2010). Niosome: A future of targeted drug delivery systems. *Journal of Advanced Pharmaceutical Technology & Research*, *1*(4), 374–380.

Khin, Y. W., & Feng, S. S. (2005). Effects of particle size and surface coating on cellular uptake of polymeric nanoparticles for oral delivery of anticancer drugs. *Biomaterials*, *26*, 2713–2722.

Kogan, A., & Garti, N. (2006). Microemulsions as transdermal drug delivery vehicles. *Advances in Colloid and Interface Science*, *123–126*, 369–385.

Kong, M., Chen, X. G., Kweon, D. K., & Park, H. J. (2011). Investigations on skin permeation of hyaluronic acid based nanoemulsion as transdermal carrier. *Carbohydrate Polymers*, *86*, 837–843.

Kong, M., Chen, X. G., & Park, H. J. (2011). Design and investigation of nanoemulsified carrier based on amphiphile-modified hyaluronic acid. *Carbohydrate Polymers*, *83*, 462–469.

Kong, M., & Park, H. J. (2011). Stability investigation of hyaluronic acid based nanoemulsion and its potential as transdermal carrier. *Carbohydrate Polymers*, *83*, 1303–1310.

Krishnaiah, Y. S. R., Satyanarayana, V., & Karthikeyan, R. S. (2002). Effect of the solvent system on the in vitro permeability of nicardipine hydrochloride through excised rat epidermis. *Journal of Pharmacy & Pharmaceutical Sciences*, *5*(2), 123–130.

Kulkarni, S. A., & Feng, S. S. (2011). Effects of surface modification on delivery efficiency of biodegradable nanoparticles across the blood–brain barrier. *Nanomedicine (London)*, *6*(2), 377–394.

Lee, J. H., Lee, Y. J., Kim, J. S., Yoon, M. K., & Choi, Y. W. (2005). Formulation of microemulsion systems for transdermal delivery of aceclofenac. *Archives of Pharmacal Research*, *28*, 1097–1102.

Liu, N., & Park, H. J. (2009). Chitosan-coated nanoliposome as vitamin E carrier. *Journal of Microencapsulation*, *26*, 235–242.

Mitragotri, S. (2004). Breaking the skin barrier: Technologies for enhancing skin permeability. *Advanced Drug Delivery Reviews*, *56*, 555–556.

Neubert, R. H. H. (2011). Potentials of new nanocarriers for dermal and transdermal drug delivery. *European Journal of Pharmaceutics and Biopharmaceutics*, *77*(1), 1–2.

Patel, R. P. (2007). *Niosomes: an unique drug delivery system*. Available from:. http://www.pharmainfo.net/reviews/niosome-unique-drug-delivery-system

Pham, T. T., Jaafar-Maalej, C., Charcosset, C., & Fessi, H. (2012). Liposome and niosome preparation using a membrane contactor for scale-up. *Colloids and Surfaces B: Biointerfaces*, *94*, 15–21.

Potts, O. R., & Francoeur, M. L. (1991). The influence of stratum corneum morphology on water permeability. *Journal of Investigative Dermatology*, *96*, 495–499.

Prausnitz, M. R., & Langer, R. (2008). Transdermal drug delivery. *Nature Biotechnology*, *26*(11), 1261–1268.

Rao, S. B., & Sharma, C. P. (1997). Use of chitosan as a biomaterial: Studies on its safety and hemostatic potential. *Journal of Biomedical Materials Research*, *34*, 21–28.

Santos, P. (2008). Application of microemulsions in dermal and transdermal drug delivery. *Skin Pharmacology and Physiology*, *21*, 246–259.

Scheuplein, R. J. (1976). Permeability of the skin: A review of major concepts and some new developments. *Journal of Investigative Dermatology*, *67*, 672–676.

Sintov, A. C., & Shapiro, L. (2004). New microemulsion vehicle facilitates percutaneous penetration in vitro and cutaneous drug bioavailability in vivo. *Journal of Control Release*, *95*, 173–183.

Sonneville-Aubrun, O., Simonnet, J.-T., & L'Alloret, F. (2004). Nanoemulsions: A new vehicle for skincare products. *Advances in Colloid and Interface Science*, *108–109*, 145–149.

Subedi, R. K., Oh, S. Y., Chun, M. K., & Choi, H. K. (2010). Recent advances in transdermal drug delivery. *Archives of Pharmacal Research*, *33*(3), 339–351.

Sun, W., Xie, C., Wang, H., & Hu, Y. (2004). Specific role of polysorbate 80 coating on the targeting of nanoparticles to the brain. *Biomaterials*, *25*(15), 3065–3071.

Thong, H. Y., Zhai, H., & Maibach, H. I. (2007). Percutaneous penetration enhancers: An overview. *Skin Pharmacology and Physiology*, *2*, 1–12.

Torchilin, V. P. (2007). Targeted pharmaceutical nanocarriers for cancer therapy and imaging. *The AAPS Journal*, *9*(2), 128–147.

Verma, D. D., Verma, S., Blume, G., & Fahr, A. (2003). Particle size of liposomes influences dermal delivery of substances into skin. *International Journal of Pharmaceutics*, *258*, 141–151.

Xia, T., Li, N., & Nel, A. E. (2009). Potential health impact of nanoparticles. *Annual Review of Public Health*, *30*, 137–150.

Zhang, L. K., Hou, S. X., Mao, S. J., Wei, D. P., Song, X. G., & Lu, Y. (2004). Uptake of folate conjugated albumin nanoparticles to the SKOV3 cells. *International Journal of Pharmaceutics*, *287*, 155–162.